Reverse Size-Dependent Electrooxidation of Gold Nanoparticles Coated with Alkanethiol Self-Assembled Monolayers (SAMs)

Badri P. Mainali, Dhruba K. Pattadar and Francis P. Zamborini*

Department of Chemistry, University of Louisville, Louisville, Kentucky 40292, United States

ABSTRACT: The oxidation potential of weakly-stabilized, citrate-coated Au and other spherical metal nanoparticles (NPs) shifts negative by an amount proportional to 1/radius due to a size-dependent negative shift in the thermodynamic standard potential, which is related to the increase in surface area-to-volume ratio (SA/V) of the NPs with decreasing size. Strongly bound stabilizers, such as alkanethiolates, provide stability by preventing aggregation in solution but also strongly influence the oxidation potential of the metal NPs. In this report, cyclic voltammetry (CV) shows that the oxidative stripping of Au by Br^- is hindered significantly for 4.1 ± 0.7 nm, 15.1 ± 1.3 nm, and 50.3 ± 1.7 nm diameter Au NPs when coated with butanethiolate (C4S), decanethiolate (C10S), and hexadecanethiolate (C16S) ligands. The resistance to oxidation increases with increasing chain length, consistent with the numerous studies on planar two-dimensional (2D) Au surfaces. When comparing sizes, the 4.1 nm alkanethiolate-coated Au NPs show greater resistance to oxidative stripping compared to the 15.1 nm and 50.3 nm diameter Au NPs coated with the same thiolates. Chronocoulometry (CC) experiments show that 15.1 and 50.3 nm diameter thiolate-coated Au NPs oxidize to a much greater extent in acidic Br^- within 1000 s at 1.0 V vs. Ag/AgCl compared to 4.1 nm Au NPs. Almost 4 times more Au dissolves from C4S-coated 50.3 nm Au NPs as compared to C4S-coated 4.1 nm Au NPs, despite the much higher surface area-to-volume ratio for the 4.1 nm Au NPs. The stability of the Au NPs against oxidation therefore has a unique reverse size-dependence for thiolate-coated Au NPs, where the extent of oxidation increases with increasing size, which is the opposite trend observed for weakly-stabilized or bare Au NPs.

INTRODUCTION

In recent years, metal nanoparticles (NPs) have drawn increasing interest due to their potential applications in the fields of catalysis,[1-2] sensing,[3] plasmonics,[4] nanoelectronics,[5] and photothermal therapy,[6] as some examples. The benefits and performance of the NPs in these applications depends on various factors, such as NP stability,[7] cytotoxicity[8] and biocompatibility.[9] Among them, stability of the NPs is a key factor that is usually determined by the type of ligand or surfactant stabilizer used in the synthesis. One common way to increase the stability is by direct adsorption of protecting ligands on the NP surfaces, which are referred to as self-assembled monolayers (SAMs).[10-11] Customarily, SAMs are comprised of ordered organic molecules adsorbed onto solid metal surfaces from the solution or gas phase.[12-13] The order and orientation of these molecular assemblies, acting as thin film coatings, play an important role in NP stability,[10, 13-14] surface functionality,[15] assembly[10, 16] and physical properties.[17] In spite of the presence of stabilizing agents, there are many examples where NPs cannot be used as intended due to their inadequate stability.[18-19]

The oxidative dissolution of metal NPs is one type of chemical instability. Several researchers previously studied the size-dependent electrochemical dissolution of metal NPs, showing that smaller-sized metal NPs oxidize (dissolve) at lower potentials compared to larger ones for sizes below about 40 nm in diameter.[20-23] Larger NPs are also typically more stable against ripening compared to smaller NPs, as demonstrated in recent constant potential measurements in halide solutions[24] and electrochemical oxidation/reduction cycling studies of different-sized Au NPs.[25-26] Based on electrochemical scanning tunneling microscopy (ECSTM), Tang *et al.* examined the electrochemical dissolution of different sized Pt-black NPs (particle radius of 0.58, 0.62, 0.83, and 1.43 nm) in acidic solution as a function of potential, where the dissolution potential decreased

with a decrease in NP size.[27] Our group recently studied the size-dependent electro-dissolution of Ag and Au NPs, where smaller NPs oxidized at lower potentials compared to larger sizes.[21, 28-29] This is generally consistent with the theory developed by Plieth, which predicts a negative shift in the standard potential of metal NPs proportional to 1/radius.[30]

The lack of proper stability of metal NPs can be an issue for many electrocatalytic applications of the NPs, such as in fuel cells.[31] For example, Trindell *et. al.* reported that 2 nm diameter Au NPs stabilized by citrate and sixth generation hydroxy-terminated polyamidoamine (G6-OH) dendrimers rapidly grew into bigger sizes when used for electrocatalytic CO_2 reduction.[32] Such instability made it impossible to correlate the electrocatalytic behavior with the NP size. Several other reports have shown that metal NPs <10 nm exhibit superior catalytic performance over bigger sizes under a variety of conditions.[1, 28, 33-36] As an example, Tang *et. al.* reported a 2.5-fold increase in kinetic current towards the oxygen reduction reaction in alkaline medium when the average size of polystyrene-block-poly(2-vinylpyridine)-stabilized Au NPs decreased from 7 nm to 3 nm in diameter.[33] Success for these applications requires strategies to enhance the stability of smaller-sized metal NPs without negatively affecting their catalytic properties. This is challenging because smaller NPs contain a larger proportion of edge and corner atoms, which are often the sites where catalytic reactions take place, but these same sites are usually less electrochemically stable. Ligand stabilizers are needed to stabilize the NPs without poisoning their catalytic properties.

Enhancing the stability of a metal, such as Au, via the assembly of organomercaptan self-assembled monolayers (SAMs) has long been practiced by several researchers.[37-39] The assembly of alkanethiols with different chain lengths onto bulk two-dimensional (2D) Au surfaces, as described in the work of Porter *et.al.*, showed that longer chain alkanethiols form more ordered

and densely-packed SAMs compared to shorter ones.[37] This was accompanied by the enhancement in surface coverage, increased packing density, and capacity to block electron transfer with longer carbon chain alkanethiols. Zamborini and Crooks studied the effect of chain length and end group of alkanethiolate SAMs on the corrosion passivation of Au in KBr solution.[40] It was observed that thiols terminated with the more hydrophilic -COOH and -OH end groups were better passivating agents against corrosion than the hydrophobic -CH_3 end groups, considering the same SAM thickness. Further, the passivation was more pronounced with SAMs having the same end group but longer carbon chain lengths due to the better organization with longer carbon chains.

We were interested in studying the barrier properties of various chain length alkanethiol SAMs assembled on 3D Au NPs against oxidative dissolution similar to the already studied 2D Au films.[41-42] Thiol ligand stabilizers are well-known for providing stability against aggregation, ripening, and oxidation (corrosion), especially for Au NPs, due to the high strength of the Au-thiolate bond.[13, 39, 43] Accordingly, different researchers have been able to develop synthetic strategies for preparing thiolate-coated Au clusters, termed monolayer-protected clusters (MPCs), ranging from 1 nm to about 5 nm in diameter.[44] MPCs 1.6 nm and below are commonly termed atomically-precise Au nanoclusters (APNCs).[45-51] The $Au_{25}(SR)_{18}^-$ (SR = organothiolate) is an example of an APNC, which incorporates 6 Au_2S_3 staple motifs around a Au_{13} cluster core.[45] Additionally, Kwak *et. al.* recently reported $Au_{25}(SR)_{18}$, $Au_{38}(SR)_{24}$, and $Au_{102}(SR)_{44}$ APNCs.[45] Negishi *et.al.* found that the growth of Au clusters during their synthesis can be suppressed by passivation with thiolates, indicating improved stability of small Au clusters with thiolates.[52] Different groups have observed the enhancement in stability of Au NPs coated with thiols.[53-55] Studies also show the replacement of citrate with thiols on citrate-stabilized Au NPs, forming

mixed citrate/thiol layers due to the stronger Au-thiolate interaction compared to the Au-citrate interaction.[56]

It is not directly clear what the effect of Au NP size will be on the oxidation of thiolate-coated Au NPs in the presence of an etchant, such as Br^-, due to a few different factors. Two potential factors predict greater oxidation with decreasing size while two other factors predict hindered oxidation with decreasing size. For the former, it is well-known from the Plieth equation,[30] Gibbs-Thomson relation,[57] and recent experimental results that the oxidation potential for metal NPs decreases as the size of the NP decreases.[21, 58] This effect is based on the surface free energy related to the exposed surface area of a sphere, taking into account the geometry only and not potential size-dependent differences in Au-thiolate adsorbate binding. Also, as the Au NP size decreases, the increased NP curvature results in alkanethiolate monolayers with high density near the Au surface, but lower density away from the surface. The alkane chains exhibit the general all-trans zigzag structure, but have greater mobility, chain folding, and a greater number of gauche defects at distances farther from the Au core.[59] The geometry-based size relation and increase in alkane chain defects with decreasing Au NP size could lead to greater amounts of oxidation with decreasing NP size. On the other hand, there are two reasons to predict a decrease in oxidation with decreasing NP size. First, the curvature and number of Au atom defects (edge and corner sites) increases with decreasing Au NP size, leading to a much higher alkanethiolate ligand coverage for monolayers on small Au NPs as compared to those on larger Au NPs or 2D Au films (>50% coverage as compared to ~33% on 2D films).[59-60] The increasing alkanethiolate coverage with decreasing size could lead to a decrease in oxidation. Second, studies have shown greater alkanethiolate monolayer electrochemical stability on NPs and highly curved surfaces compared to 2D planar surfaces.[61] This is due to a shorter and stronger Au-thiolate bond on the high energy

surfaces of the smaller Au NPs, which contain a larger number of atomic defects.[60, 62] Au NPs accordingly exhibit a contraction in the Au-Au lattice with decreasing size, especially below ~4 nm, which is relaxed upon strong binding with alkanethiolate monolayers to reduce the overall surface stress.[60] It is therefore possible that stronger alkanthiolate bonding to smaller Au NPs would lead to a lower surface energy and less oxidation compared to larger Au NPs with the same alkanethiolates.

Clearly there are two possible factors leading to increased oxidation with decreasing Au NP size (geometric surface area and alkane chain defects) and two reasons to expect decreased oxidation with decreasing Au NP size (ligand density and reduced surface energy due to stronger Au-thiolate bonding), making this an important topic to explore. It is also important to consider that some of the effects would alter the thermodynamics of oxidation, such as those involving changes in surface free energy (geometry and Au-thiolate binding), while others would more likely alter the oxidation kinetics, such as ligand density and chain defect density. Different amounts of ligand density and chain defects could sterically alter access of the etchant to the Au surface. Accordingly, we here describe the electrochemical oxidation of electrode-attached, citrate-stabilized 4.1 nm, 15.1 nm, and 50.3 nm diameter Au NPs 1) as-prepared and 2) following modification with butanethiolate (C4S), decanethiolate (C10S), and hexadecanethiolate (C16S) SAMs. We compare the oxidative dissolution of citrate- and alkanethiolate-modified Au NPs as a function of size in acidic Br^- electrolyte by cyclic voltammetry (CV), chronocoulometry (CC), and UV-Vis spectro-electrochemistry.

EXPERIMENTAL

Chemicals and Reagents. $HAuCl_4 \cdot 3H_2O$ was synthesized from 99.99% metallic Au in our lab by first cleaning the Au in 3:1 hydrogen peroxide : sulfuric acid ("piranha") , rinsing thoroughly with water, dissolving in 3:1 hydrochloric acid : nitric acid solution ("aqua-regia"), performing 4 distillations, where we replaced the distilled aqua regia with concentrated hydrochloric acid, and finally crystallizing to form the solid complex by gentle heating in a crystallization dish (aqua-regia and piranha are highly hazardous to the skin or when inhaled and were handled with high precaution!). Sodium borohydride, (3-aminopropyl)triethoxysilane (≥98.0%), hydrogen peroxide solution (30 wt.%, ≥98.5 reagent grade), 2-propanol (ACS reagent), 1-butanethiol (C4S, 99 %), 1-decanethiol (C10S, 96%), and 1-hexadecanethiol (C16S, 92% tech), were purchased from Sigma Aldrich and used as received. Trisodium citrate salt (Bio-Rad laboratories), potassium perchlorate (Beantown Chemical, 99.0-100.5%), potassium bromide (EMD, GR ACS), and perchloric acid (Merck, 60%) were used as received. Hydrochloric acid (ACS, 36.5-38%), sulfuric acid (ACS, 95-98%), and nitric acid (ACS, 68-70%) were purchased from VWR. Ethyl alcohol (ACS/USP grade) and acetone (ACS/USP grade) were purchased from Pharmco-AAPER and used as received. All aqueous solutions were prepared from water purified with a Barnstead NANO purification system having a resistivity of 18.2 MΩ-cm.

Chemical Synthesis of Citrate-Stabilized Au Nanoparticles (NPs). 4.1 ± 0.7, 15.1 ± 1.3 and 50.3 ± 1.7 nm average diameter citrate-stabilized Au NPs were prepared as described by our groups in several previous publications,[63-64] based on the methods adopted by Murphy and co-workers,[65] Turkevich *et al.*,[66] and Wang and coworkers,[67] respectively. The methods involve the reduction of $HAuCl_4 \cdot 3H_2O$ in the presence of trisodium citrate using sodium borohydride, high temperature, and hydrogen peroxide for the 4.1 nm, 15.1 nm, and 50.3 nm Au NPs, respectively. The synthesis of 50.3 nm Au NPs occurs by seed-mediated growth of 15.1 nm diameter Au NPs.

The final color of the solutions were red for 4.1 nm and 15.1 nm Au NPs and a pink-red for the 50.3 nm Au NPs. The Au NP solutions were freshly-prepared for all experiments and used as prepared within 2 hours to obtain reproducible results.

Functionalization of Glass/ITO Electrodes with Au NPs. Attachment of all Au NPs to indium-tin-oxide-coated glass electrodes (glass/ITO) was performed as described by our group in a number of publications.[24, 64] Glass/ITO electrodes (CG-50IN-CUV, R_s = 8-12 Ω, 2.5 cm x 0.7 cm) were purchased from Delta Technologies, Limited (Loveland, CO). The electrodes were cleaned by sonication for 30 min each in acetone, ethanol, and 2-propanol and then dried under N_2. The glass/ITO electrode was then functionalized with (3-aminopropyl)triethoxysilane (APTES) by immersing into a solution containing 100 μL of APTES, 10 mL of 2-propanol, and 2 to 3 drops of nanopure water and heating at 70-80 ^oC for 30 min. After 30 min, the electrode was thoroughly rinsed with 2-propanol and dried under N_2. The glass/ITO/APTES electrodes were placed into as prepared or diluted Au NP solutions to obtain the desired coverage of Au NPs on the electrode surface. Care was taken to maintain the same total amount of Au on the electrode surface for the different-sized Au NPs by soaking them for different times and having different concentrations of Au NPs through dilution (4.1 nm: 3-5 min in 3-fold dilute solution, 15.1 nm: 8-10 min in direct solution, 50.3 nm: 25-30 min in direct solution).

After soaking the glass/ITO/APTES in an Au NP solution, the electrodes were rinsed thoroughly with nanopure water, dried under N_2, and then the Au coverage was determined by electrochemically measuring the surface area (SA) from the Au oxide reduction peak in a cyclic voltammogram (CV) obtained in 0.1 M $HClO_4$ electrolyte and determining the volume (V) from the known SA/V ratio for each size Au NPs.[64] The total V of Au NPs measured in this way is directly proportional to the total amount of Au attached to the glass/ITO/APTES electrode. If the

V did not reach a specific pre-determined value, the electrode was rinsed with nanopure water, dried under N_2, and placed back into the Au NP solution for more time. The target integrated Coulombs under the Au oxide reduction peak from CV (proportional to total Au SA) was ~3.4 x 10^{-5} Coulombs, ~1.3 x 10^{-5} Coulombs, and ~3.5 x 10^{-6} Coulombs for the 4.1 nm, 15.1 nm, and 50.3 nm Au NPs, respectively. Once reached, the samples were rinsed with nanopure water, dried under N_2 and then either analyzed directly or functionalized with the alkanethiol of interest. Electrodes that did not fall into the pre-determined Au coverage range were discarded and not included in the statistics.

Deposition of Alkanethiolate Self-Assembled Monolayers on the Au NPs. Following Au NP attachment to glass/ITO/APTES at the appropriate Au coverage, samples were functionalized with alkanethiols by soaking in a 200 proof ethanolic solution of 2 mM C4S, C10S and C16S alkanethiol overnight. The samples were removed from solution, thoroughly rinsed with 200 proof ethanol, and finally dried under N_2 before immediate electrochemical analysis.[10, 12]

Au NP Characterization. Scanning electron microscopy (SEM) images of different-sized Au NPs attached to glass/ITO/APTES were obtained at different magnifications using a Carl Zeiss SMT AG SUPRA 35VP field emission scanning electron microscope (FESEM) operating at an accelerating voltage of 15.00 kV and using an in-lens ion annular secondary electron detector. Ultraviolet-visible spectrometry (UV-Vis) was performed using a Varian instrument, model Cary 50 Bio-spectrophotometer. UV-Vis spectra for different sized Au NPs were obtained in a visible light range of 400-750 nm. The corresponding absorbance values were normalized to a value of 1.0 at 400 nm.

Electrochemical and Spectroelectrochemical Characterization. A CH Instruments (Austin, TX) model CHI660E electrochemical workstation consisting of a 3-electrode set-up with the

glass/ITO/APTES/Au NPs as working electrode, a Pt wire as the counter electrode, and an Ag/AgCl (3 M KCl) as the reference electrode was used to perform cyclic voltammetry (CV), anodic stripping voltammetry (ASV) and chronocoulometry (CC). Electrolyte of 0.1 M $HClO_4$ was used for CV measurements, which were obtained at a scan rate of 0.1 V/s from a starting potential of 0 V to a final potential of 1.6 V. For CC measurements, the electrolyte was 0.01 M KBr plus 0.1 M $HClO_4$ with an initial potential of 0.0 V and a final potential of 1.0 V or 1.2 V at a pulse width of 1000 s. ASV was performed from 0.0 V to 1.2 V or 1.4 V in 0.01 M KBr plus 0.1 M $KClO_4$ at a scan rate of 0.01 V/s. For spectroelectrochemical measurements, all three electrodes were fixed inside a 1 cm path length plastic cuvette in the sample holder of the UV-Vis instrument, with an electrolyte solution of 0.01 M KBr plus 0.1 M $HClO_4$. CC was performed as already described and the localized surface plasmon resonance (LSPR) peak of the electrode attached Au NPs was monitored as a function of time and potential. A decrease in the LSPR peak intensity indicated dissolution of the Au NPs.

RESULTS AND DISCUSSION

General Experimental Set-up. In this study, we synthesized three different sized citrate-coated Au NPs with average diameters of 4.1 ± 0.7, 15.1 ± 1.3, and 50.3 ± 1.7 nm as described by our group previously.[28] As shown in Scheme 1, the citrate-coated Au NPs were first synthesized (Step 1) and then electrostatically attached to glass/ITO/APTES

Scheme 1: General experimental procedure in this work

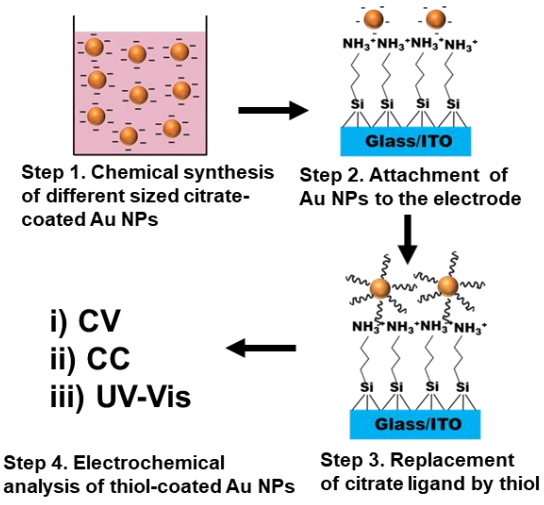

electrodes by simply soaking the electrodes into the aqueous solutions of the Au NPs (Step 2). Next, the glass/ITO/APTES/Au NPs were coated with different alkanethiol self-assembled monolayer (SAMs), where presumably a large portion of the citrate ligands become replaced by thiolates (Step 3).[56] Finally, we characterized the relative oxidation behavior of the different-sized thiol-coated Au NPs by cyclic voltammetry (CV), chronocoulometry (CC), and UV-Vis spectroelectrochemistry (Step 4) and compared the results to those of citrate-coated Au NPs.

Characterization of Au NPs. The synthesized Au NPs were characterized by UV-vis spectroscopy in solution and by scanning electron microscopy (SEM) after attachment to glass/ITO/APTES electrodes. Figure S1 shows the results, which is fully consistent with these same sized Au NPs synthesized and characterized by our group previously.[24, 64]

Constant Coverage of Au NPs. In order to compare the stability of the different-sized, electrode-attached citrate and thiol-coated Au NPs towards oxidative dissolution, it is important to keep the total coverage (in terms of Au atoms) constant on the electrode surface. In order to do this, we first subjected the electrode-attached Au NPs to cyclic voltammetry (CV) in 0.1 M $HClO_4$ from 0 V to 1.6 V vs Ag/AgCl. This provides information about the oxidation-reduction behavior of the surface Au atoms. In the first positive scan, Au becomes oxidized to AuO_x, possibly as Au_2O_3, while in the negative scan of the cycle, Au_2O_3 is reduced back to metallic Au (Equation 1) at around 0.80 V for all Au NPs in this study. The integrated charge obtained from the Au oxide reduction peak at 0.80 V is proportional to the total surface area (SA) of the Au NPs since it only involves oxide formation of the surface Au atoms. By knowing the total SA experimentally and using the previously measured surface area-to-volume (SA/V) ratio for the different sized Au NPs,[64] we were able to determine the total volume (V) of Au for the different sized Au NPs on glass/ITO/APTES. The total V is directly proportional to the coverage in terms of Au atoms.

Based on our previous work, the average SA/V ratio is 0.64, 0.23 and 0.060 for 4.1, 15.1 and 50.3 nm Au NPs, respectively (not cleaned with ozone).[64] From this value, we were able to calculate the expected total V of Au (target of 5.70×10^{-5} C) by dividing the electrochemically-measured SA by the previously reported SA/V,[64] which gave target SA values of 3.4×10^{-5} C, 1.3×10^{-5} C, and 3.6×10^{-6} C for 4.1 nm, 15.1 nm, and 50.3 nm diameter Au NPs, respectively. Figure S2 shows an examples of 3 samples, where the SA values were 3.30×10^{-5}, 1.29×10^{-5} and 3.48×10^{-6} Coulombs of integrated charge for the reduction peak at 0.80 V, which resulted in ASV coverages (or V) obtained in 0.01 M KBr plus 0.1 M $KClO_4$ of 5.55×10^{-5}, 5.63×10^{-5}, and 5.76×10^{-5} Coulombs for 4.1, 15.1 and 50.3 nm Au NPs, respectively. Table S1 shows the integrated charges (in Coulombs) of glass/ITO/APTES/Au NP electrodes obtained from the Au oxide reduction peak in 0.1 M $HClO_4$ and the oxidative charge from the 1st scan of the ASV in 0.01 M KBr plus 0.1 M $KClO_4$. Likewise, Table S2 shows the experimentally-measured integrated SA coverages of the different-sized Au NPs and the corresponding calculated V of all the samples used (using the SA/V from our previous work)[64] for the CV and CC experiments in this work.

$$Au_2O_3 + 6H^+ + 6e^- \leftrightharpoons 2Au + 3H_2O \qquad (1)$$

$$Au^0 + 4Br^- \longrightarrow AuBr_4^- + 3e^- \ (E^0 = 0.85 \text{ V vs NHE}) \qquad (2)$$

$$Au^0 + 2Br^- \longrightarrow AuBr_2^- + e^- \ (E^0 = 0.96 \text{ V vs NHE}) \qquad (3)$$

Stability Against Oxidation as Measured by CV. To analyze the stability of citrate- and alkanethiolate-coated Au NPs, we performed CV experiments in the presence of 0.01 M KBr plus 0.1 M $HClO_4$, where Br^- was used to oxidize Au from the electrode surface, forming soluble $AuBr_4^-$ and $AuBr_2^-$ complexes as shown in reactions 2 and 3. Figure S3A shows CVs of citrate-coated 4.1 nm, 15.1 nm, and 50.3 nm Au NPs having similar volume on the electrode surface taken in 0.01

M Br^- plus 0.1 M $HClO_4$ solution at a scan rate of 0.1 V/s. The oxidation peak potential ($E_{p,ox}$) appears at 0.96 V, 0.86 V, and 0.80 V for the 50.3 nm, 15.1 nm, and 4.1 nm diameter Au NPs, respectively, which agrees with the well-known decrease in peak oxidation potential with decreasing size described by us and others in the literature.[23, 29] Next, we determined the stability of the different sized alkanethiolate-coated Au NPs by monitoring their trend of oxidation in the

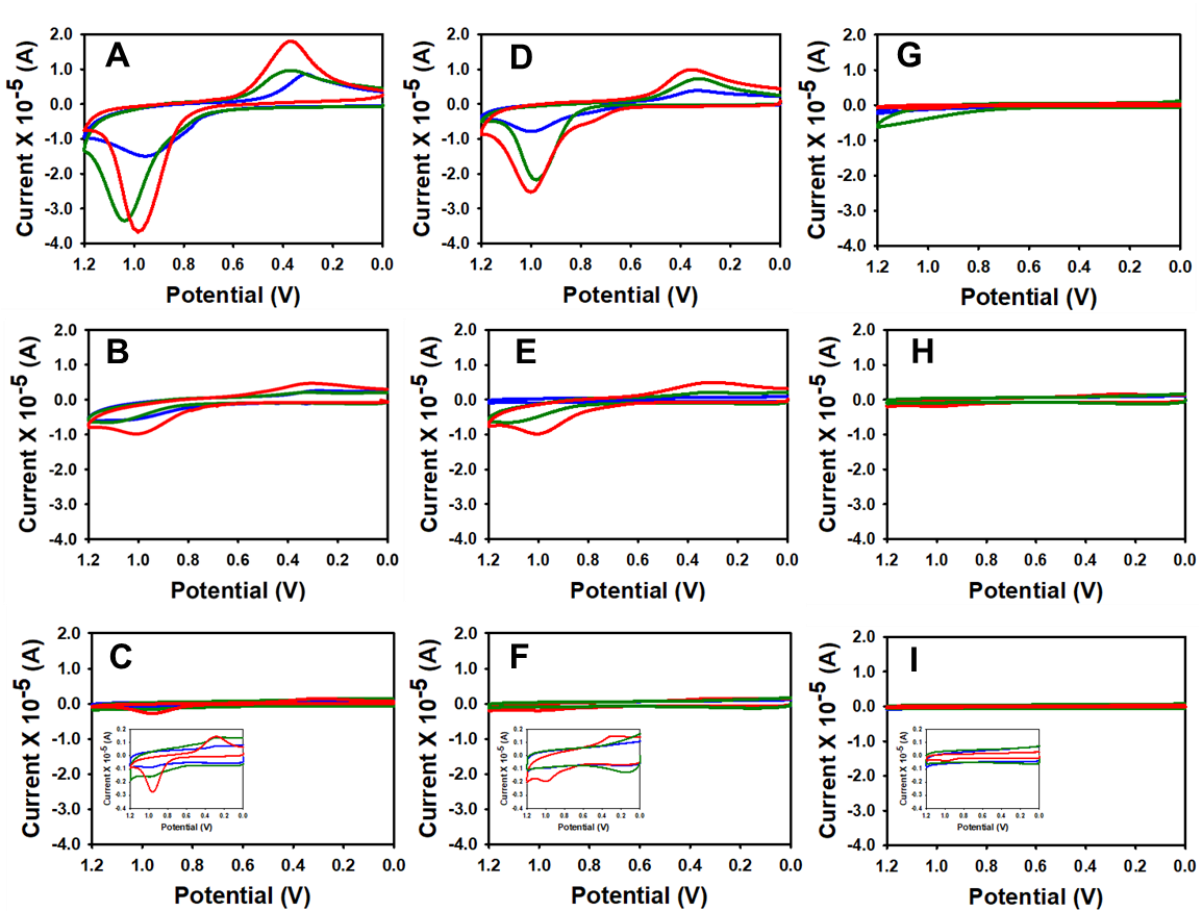

Figure 1. Cyclic voltammograms (CVs) obtained from 0.0 to 1.2 V in 0.01 M KBr and 0.1 M $HClO_4$ of glass/ITO/APTES electrode with 4.1 nm (blue), 15.1 nm (green) and 50.3 nm (red) Au NPs coated with C4S (1st column, A-C), C10S (2nd column, D-F) and C16S (3rd column, G-I) alkanethiol SAMs. Rows 1, 2 and 3 represent the 1st, 5th and 50th CV scans respectively. Frames C, F and I having low oxidation-reduction current level are blown up 10 times as included in the inset for more visibility of the current.

Br^--containing acidic electrolyte. The relative stability of Au NPs coated with alkanethiolate SAMs was studied by comparing the current observed for the reduction of $AuBr_4^-/AuBr_2^-$ during

the reverse negative scan of the CV (Figure 2) rather than the oxidation peak, since Br^- oxidation to Br_2 can occur near the Au oxidation peak. On the 1st CV scan, there was a significant amount of reduction current for 4.1 nm, 15.1 nm, and 50.3 nm C4S-coated Au NPs (Figure 1A). C4S-coated 4.1 nm Au NPs showed the least amount of current while the 15.1 nm was intermediate and 50.3 nm Au NPs showed the most current. This suggests that more Au dissolved from the 50.3 nm Au NPs, indicating that the C4S passivated them the least. We continued scanning up to 50 CV cycles. On the 5th scan (Figure 1B), there was still slightly more reduction current for the 50.3 nm Au NPs compared to the 15.1 nm and 4.1 nm Au NPs. The peak current for Au reduction gradually decreased and was significantly low by the 50th scan (Figure 1C) for all sizes. The close to disappearance of the reduction peak is due to the eventual complete oxidative dissolution of all Au NPs, where the Au fully dissolved (except the tiny peak for 50.3 nm) and diffused away from the electrode surface, where it could no longer be re-reduced. The overall behavior indicates that C4S-coated 4.1 nm Au NPs are more resistive to dissolution by Br^- than the bigger-sized C4S-coated 15.1 nm and 50.3 nm Au NPs. This trend is opposite of what occurred for citrate-coated 4.1 nm, 15.1 nm, and 50.3 nm Au NPs, where $E_{p,ox}$ increased with increasing size on the first scan (Figure S3A), while the stripping charge was similar (Table S1). The re-reduction charge was 40%, 46%, and 30% of the oxidation charge for the 50.3, 15.1, and 4.1 nm Au NPs, respectively, as shown in Table S1 (reduction peak charge divided by oxidation peak charge). The smaller re-reduction charge for 4.1 nm Au NPs in this case is not due to greater stability. The reduction charge is somewhat complicated by higher mass transport away from the smaller Au NPs, longer time for $AuBr_4^-/AuBr_2^-$ ions to diffuse away for smaller Au NPs due to lower $E_{p,ox}$, and earlier times for re-reduction of $AuBr_4^-/AuBr_2^-$ due to higher overpotentials for reduction on larger Au NPs (more negative reduction potential on 50.3 nm Au NPs). Nevertheless, by the 50th CV scan (Figure S3C),

all the Au clearly dissolved and diffused away for 4.1 nm and 15.1 nm, while there remained a small amount of undissolved Au for 50.3 nm NPs, showing greater stability for the largest size Au NPs.

We next performed similar measurements with the same three Au NPs but coated with C10S (Figure 1D-1F) and C16S (Figure 1G-1I) SAMs, where again the smallest size 4.1 nm diameter Au NPs showed the smallest reduction peak current (blue plot) while the largest 50.3 nm Au NPs showed the largest reduction peak current (red plot). The 5th scan showed the same trend while very low reduction peak current appeared for all Au NPs on the 50th scan, indicating very little Au dissolution occurring at that point. This data again shows that the 4.1 nm Au NPs are more passivated by alkanethiolates than the 15.1 nm and 50.3 nm Au NPs. Figure 1G shows the 1st CV scan of the different sized Au NPs coated with the longest C16S thiolate SAMs. Unlike C4S and C10S SAMs, the reduction peak current in this case is negligible for all the Au NP sizes on the 1st scan, indicating very little Au dissolution for any of them. Upon continued CV scanning, the reduction peak current remained negligible on the 5th scan (Figure 1H) and very small on the 50th scan as well (Figure 1I), although there are very small peaks o bserved for 50.3 nm and 15.1 nm Au NPs on the 50th scan as shown in the inset with the current scale blown up 10 times. This is again consistent with less passivation for the larger Au NPs. This data also indicates stronger passivation against dissolution for all sized Au NPs as the alkanethiolate chain length increases from C4S to C16S, which is consistent with what has been observed previously on 2D Au electrodes.[40, 53, 68] The CVs in Figure 2 clearly show the significant effect of chain length of the alkanethiolates on the oxidation behavior of the different-sized Au NPs on the 1st CV scan.

Stability Against Oxidation Measured by CC. As mentioned, the reduction current in the CVs can be complicated by diffusion of soluble species away from the surface upon dissolution as

well as different times between oxidation and reduction potentials. Also, it is not clear that a lack of a reduction peak is indicative of passivation or complete dissolution of Au on later scans. In order to resolve this confusion, we used chronoco ulometry (CC) to further confirm the relative stability of different-sized Au NPs coated with alkanethiolate SAMs. CC of alkanethiolate-coated Au NPs was performed by holding the potential of the working electrode at 1.0 V for 1000 sec in 0.01 M KBr plus 0.1 M $HClO_4$. As shown in the CC plots of citrate-coated 4.1 nm, 15.1 nm, and 50.3 nm Au NPs (Figure 3A), this potential oxidizes more than 90% of the Au for all Au NP sizes within 500 sec and we successfully maintained a similar amount of Au for each size on the electrode based on the final charge of 600-750 μC for the citrate-coated Au NPs (Figure 3A). Figure 3B-3D show the CCs of 4.1 nm, 15.1 nm, and 50.3 nm Au NPs coated with C4S, C10S, and C16S SAMs, respectively. In all cases, the total stripping charge is lowest for the 4.1 nm diameter Au NPs compared to the 15.1 nm and 50.3 nm Au NPs, consistent with the strongest passivation of the smallest Au NPs. The C4S SAMs passivated the 15.1 nm Au NPs more effectively compared to 50.3 nm Au NPs, while C10S and C16S were similar for 15.1 nm and 50.3 nm Au NPs. Figure 4 summarizes the CC data, where the average stripping charge was not

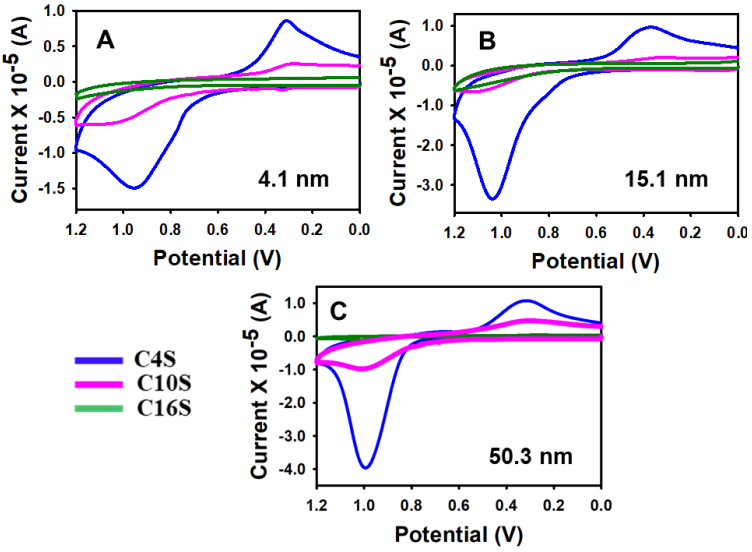

Figure 2. Cyclic voltammetry (1st scan) of 4.1, 15.1 and 50.3 nm Au NPs in C4S (blue), C10S (pink) and C16S (green) alkanethiol SAMS in 0.01 M KBr and 0.1 M $HClO_4$ showing the significant effect of alkanethiol C-chain length on electrooxidation of Au NPs.

significantly different for citrate coated Au NPs of all sizes (520-620 μC). They also were not significantly different for C16S coated Au NPs (all <100 μC), since all 3 sizes were well passivated. For C4S-coated Au NPs, the 4.1 nm Au NPs showed a significantly lower stripping charge (~100 μC) followed by 15.1 nm Au NPs (~200 μC) and finally 50.3 nm Au NPs (~350 μC). For C10S-coated Au NPs, only the 4.1 nm Au NPs showed significantly lower stripping charge (~50 μC) compared to the 15.1 nm and 50.3 nm Au NPs (~100 μC).

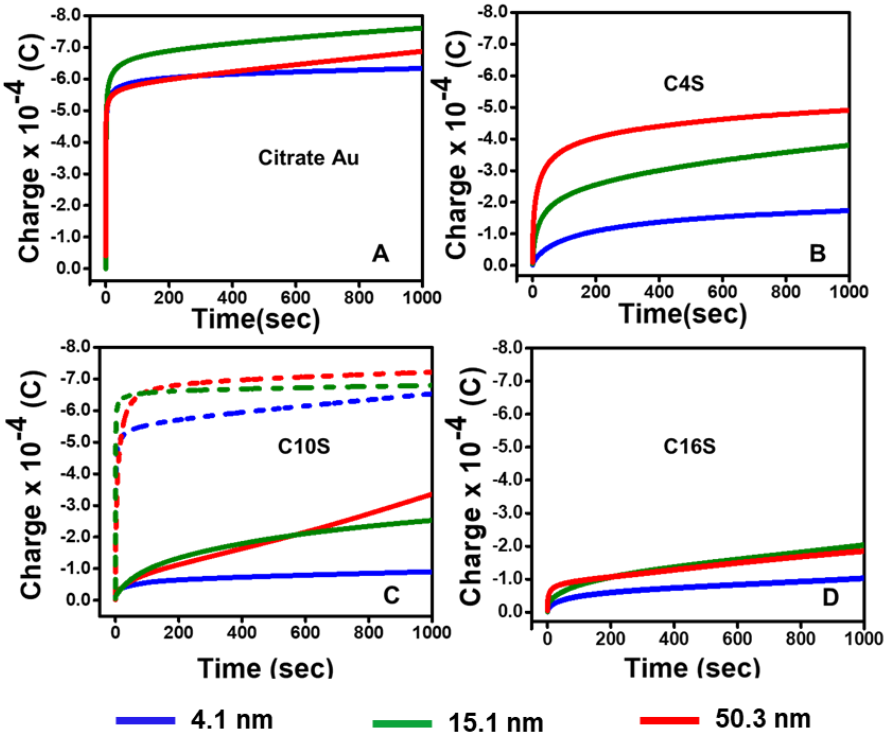

Figure 3. Chronocoulometry of 4.1 nm (blue), 15.1 nm (dark green) and 50.3 nm (red) Au NPs in 0.01 M KBr and 0.1 M $HClO_4$ at 0.0 to 1.0 V taken for 1000 seconds. A) Citrate Au NPs B) Au NPs in C4S C) Au NPs in C10S D) Au NPs in C16S alkanethiol SAMs. Dashed lines with matching color in plot C represent the corresponding CC of Au NPs in C10S alkanethiol SAMs followed by 30 min ozone treatment.

One possible reason for the different stripping charge for the different sized Au NPs in the CC plots could be that the thiols dissolve some of the Au NPs during assembly. If they dissolve the 4.1 nm Au NPs more readily during assembly, then this could explain the reason for the lower stripping charge for the 4.1 nm Au NPs. To rule this possibility out, we attached a similar amount of different sized Au NPs on to the electrode surface and formed SAMs of C10S as already described. We then treated all of the samples with ozone for 30 min, which removes the thiolate

ligands from the Au NP surfaces as reported previously.[69] We then performed CC, with the results shown in Figure 3C (dashed plots) and Figure 4. Since the charge is statistically the same as the citrate coated Au NPs, this conclusively shows that the thiol self-a ssembly does not dissolve any Au significantly and does not itself alter the amount of Au on the surface. This confirms that the thiol SAMs do passivate the smaller Au NPs more effectively than the larger Au NPs. The CC results in Figures 3 and 4 agree well with the CV results in Figures 1 and 2 but are more conclusive.

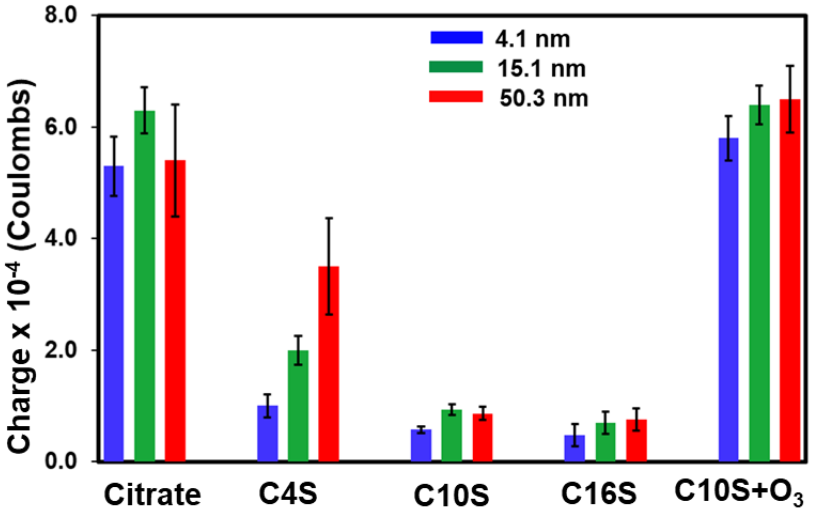

Figure 4. Box plot showing the average of charges along with standard deviation obtained in CC for 4.1 nm (blue), 15.1 nm (dark green) and 50.3 nm (red) citate coated Au NPs and those after treatment with C4S, C10S and C16S alkanethiol SAMs. Far right side of the plot diagram represents the average of CC charges of Au NPs in C10S thiol SAMs followed by 30 min of ozone treatment.

To further explore the passivating ability of SAMs as a function of Au NP size, we soaked glass/ITO/APTES/Au NP electrodes, having the same total amount of Au but different size Au NPs, in C4S to form the SAM coatings. Next, we performed CC by stepping from 0.0 V to 1.0 V in 0.01 M KBr plus 0.1 M $HClO_4$ for 400 s. As shown in Figure S4A, the charge due to Au oxidation decreased as the size of the Au NPs decreased, similar to the results in Figure 3B and Figure 4. Following the CC, we removed the electrodes from the electrochemical cell, rinsed with nanopure water, and dried under nitrogen. Then we treated the samples with ozone for 30 min to

remove any C4S remaining on the Au NPs. Finally, we performed ASV in 0.01 M KBr and 0.1 M $KClO_4$ to determine how much Au was left on each of the electrodes. As shown in Figure S4B, we observed that the Au oxidation peak size followed the order of 4.1 nm > 15.1 nm > 50.3 nm Au NPs. The average integrated ASV charge was 29.0 ± 3.1 μC, 15.7 ± 2.6 μC, and 9.7 ± 0.1 μC for the 4.1 nm, 15.1 nm, and 50.3 nm Au NPs, respectively (n=3). The larger Au oxidation peak shows that there was less Au dissolution during the CC experiment for 400 s at 1.0 V. This confirms that the C4S passivated the smaller 4.1 nm diameter Au NPs the most effectively.

Spectroelectrochemical Characterization. The size-dependent oxidative stripping of citrate-stabilized and thiolate-coated Au NPs was monitored by measuring the decrease in absorbance of the Au localized surface plasmon resonance (LSPR) extinction band in the UV-Vis region in a spectroelectrochemical set up. The absorbance was measured of the glass/ITO/APTES/Au NPs electrodes against a glass/ITO/APTES blank at 1.0 V vs. Ag/AgCl in 0.01 M KBr plus 0.1 M $HClO_4$ at various times. Strong optical absorbance requires a high coverage of all sized Au NPs on the electrode surface which we obtained by soaking functionalized glass/ITO/APTES into the as-prepared solution of Au NPs for different time (4.1 nm – 2 hr, 15.1 nm – 3 hr, 50.3 nm – 5 hr) so that the color of the Au NPs attached onto the electrode was visible. Under high coverage, Au NPs clearly showed the LSPR band at different positions than expected for solution-phase NPs, but importantly we were able to observe a decrease in the LSPR peak absorbance as a function of time in order to monitor the oxidation at 1.0 V or 1.2 V (Figure 5A, 5B, and S5). Figure 5C shows a plot of the normalized absorbance of the LSPR peak (λ_{max}) for citrate-coated 4.1 nm, 15.1 nm, and 50.3 nm Au NPs during CC in 0.01 M KBr plus 0.1 M $HClO_4$ solution at 1.0 V vs Ag/AgCl. We observed that the normalized absorbance decreased relatively fast for all sized Au NPs indicating that these NPs have low stability against oxidation in Br^- at 1.0 V. The 4.1 nm and 15.1

nm Au NPs dissolved faster compared to the 50.3 nm Au NPs, showing a decrease in normalized absorbance from 1.0 to 0.0 within 500 s for the former as compared to 700 s for the latter. This is consistent with the greater stability of larger-sized citrate-stabilized Au NPs.[28-29] Figure 5D shows the decrease in normalized absorbance at ~540 nm for C4S-coated Au NPs as a function of time. In this case, the absorbance decreased faster for the 50.3 nm Au NPs than the smaller sized 15.1 nm and 4.1 nm Au NPs. Consistent with the CV and CC results, this trend is opposite to the trend exhibited by citrate-coated Au NPs, showing again that the smaller-sized 4.1 nm Au NPs are significantly more stable when coated with C4S SAMs than the 15.1 nm or 50.3 nm Au NPs. Similar behavior was observed for Au NPs coated with C10S thiols (Figure 5E) and C16S thiols (Figure 5F). In order to confirm whether all the Au on the electrode was oxidized or not when coated with the longer chain alkanethiolate SAMs (C10S and C16S), we switched the CC potential to 1.2 V beyond 1000

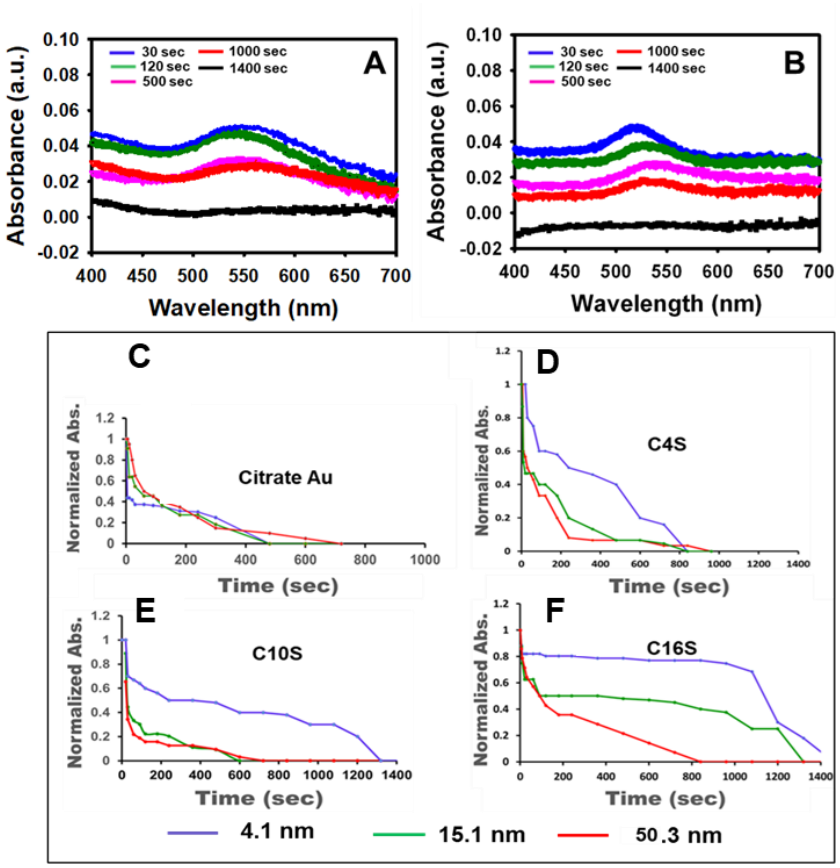

Figure 5. Chronocoulometry of 4.1 nm (blue), 15.1 nm (green) and 50.3 nm (red) Au NPs in electrolytes of 0.01 M KBr and 0.1 M $HClO_4$ at 0.0 to 1.0 V taken up to 1400 s. A) Bare Au NPs, B) Au NPs in C4S, C) Au NPs in C10S, D) Au NPs in C16S alkanethiolate SAMs. The CC operating potential was set at 1.0 V up to 1000 s and at 1.2 V between 1000 to 1400 s.

s. We found that the absorbance value decreased significantly for the 4.1 nm Au NPs when we continued at 1.2 V for an additional 400 s, confirming that more Au existed on the electrode surface after the first 1000 s (Figures 5E and 5F). In contrast, the normalized absorbance did not decrease further for C10S-coated 15.1 nm and C10S-coated or C16S-coated 50.3 nm Au NPs, confirming that those Au NPs had already fully dissolved in the first 1000 s. The C16S-coated 15.1 nm Au NPs did not completely dissolve within 1000 s, so we continued oxidizing them for another 400 sec at 1.2 V. We observed that at 1300 s total, the normalized absorbance decreased significantly (Figure 5F). All UV-Vis spectra with time are shown in Figure S5. The spectroelectrochemical data clearly support our conclusion of a reverse size-dependent stability of alkanethiolate-stabilized Au NPs compared to citrate-stabilized Au NPs.

CONCLUSIONS

CV, CC, and spectroelectrochemical experiments all reveal the trend in size-dependent oxidation of Au NPs coated with alkanethiolates, where oxidation is surprisingly more pronounced on larger-sized Au NPs. This is opposite of the behavior of Au NPs stabilized with more weakly-bound citrate ligands, which show more pronounced oxidation on smaller-sized Au NPs in agreement with the thermodynamic size prediction by Plieth.[30] While the reasons are not conclusively known, we believe the higher defect, lower coordination Au atoms on the surface of smaller Au NPs promotes stronger binding to alkanethiolates, which results in reduced surface energy and stronger passivation against oxidative dissolution in Br^-. This effect appears to be more important than the lower ordering of the alkane chains when assembled on smaller, high curvature 3D Au nanocrystals and more important than the lower thermodynamic stability of small Au NPs due to their higher surface area-to-volume ratio (SA/V). The stronger Au-S binding evens things out thermodynamically and actually provides higher stability for smaller Au NPs relative to larger

Au NPs. Future studies will explore sub 4 nm diameter Au NPs and different types of ligand stabilizers. Optimization of NP stabilizers to provide high metal stability but also strong reactivity in terms of catalysis or sensing is crucial. Our methods are useful for better understanding metal NP oxidative stability as a function of size and stabilizer to render them useful for future applications.

SUPPORTING INFORMATION

UV-Vis and SEM characterization of Au NPs, CV and ASV plots having different SA but similar volume, CV of citrate-coated Au NPs upon stripping, CC of C4S coated Au NPs followed by O_3 treatment and stripping of Au NPs by ASV, and raw UV-Vis data as a function of time and potential during CC experiments is provided in Figures S1 through S5. Integrated CV and ASV charges under different conditions are given in Tables S1 and S2.

AUTHOR INFORMATION

Corresponding Author

*E-mail: f.zamborini@louisville.edu

Notes: The authors declare no competing financial interest.

ACKNOWLEDGMENTS

We gratefully acknowledge the National Science Foundation (NSF) for financial support of this research through grants CHE-1611170 and CHE-2004169.

TOC FIGURE:

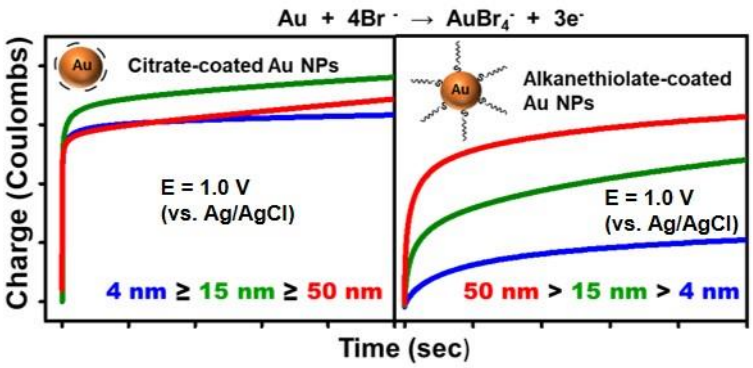

REFERENCES:

1. Mistry, H.; Reske, R.; Zeng, Z.; Zhao, Z.-J.; Greeley, J.; Strasser, P.; Cuenya, B. R., Exceptional Size-Dependent Activity Enhancement in the Electroreduction of CO2 over Au Nanoparticles. *J. Am. Chem. Soc.* **2014,** *136*, 16473-16476.
2. Ostojic, N.; Crooks, R. M., Electrocatalytic Reduction of Oxygen on Platinum Nanoparticles in the Presence and Absence of Interactions with the Electrode Surface. *Langmuir* **2016,** *32*, 9727-9735.
3. Ibañez, F. J.; Zamborini, F. P., Chemiresistive Sensing of Volatile Organic Compounds with Films of Surfactant-Stabilized Gold and Gold−Silver Alloy Nanoparticles. *ACS Nano* **2008,** *2*, 1543-1552.
4. Fang, A.; White, S.; Jain, P. K.; Zamborini, F. P., Regioselective Plasmonic Coupling in Metamolecular Analogs of Benzene Derivatives. *Nano Lett.* **2015,** *15*, 542-548.
5. Homberger, M.; Simon, U., On the Application Potential of Gold Nanoparticles in Nanoelectronics and Biomedicine. *Philosoph. Transac. Royal Soc. A* **2010,** *368*, 1405-1453.
6. Hornos Carneiro, M. F.; Barbosa, F., Gold nanoparticles: A critical review of therapeutic applications and toxicological aspects. *J. Toxico. Env. Health* **2016,** *19*, 129-148.
7. Wang, Y.; Van de Vyver, S.; Sharma, K. K.; Roman-Leshkov, Y., Insights into the stability of gold nanoparticles supported on metal oxides for the base-free oxidation of glucose to gluconic acid. *Green Chem.* **2014,** *16*, 719-726.
8. Deng, J.; Yao, M.; Gao, C., Cytotoxicity of gold nanoparticles with different structures and surface-anchored chiral polymers. *Acta Biomater.* **2017,** *53*, 610-618.
9. Pauksch, L.; Hartmann, S.; Rohnke, M.; Szalay, G.; Alt, V.; Schnettler, R.; Lips, K. S., Biocompatibility of silver nanoparticles and silver ions in primary human mesenchymal stem cells and osteoblasts. *Acta Biomater.* **2014,** *10*, 439-449.
10. Love, J. C.; Estroff, L. A.; Kriebel, J. K.; Nuzzo, R. G.; Whitesides, G. M., Self-Assembled Monolayers of Thiolates on Metals as a Form of Nanotechnology. *Chem. Rev.* **2005,** *105*, 1103-1170.
11. Huang, R.; Carney, R. P.; Stellacci, F.; Lau, B. L. T., Colloidal Stability of Self-Assembled Monolayer-Coated Gold Nanoparticles: The Effects of Surface Compositional and Structural Heterogeneity. *Langmuir* **2013,** *29*, 11560-11566.
12. Cavalleri, O.; Gilbert, S. E.; Kern, K., Growth manipulation in electrodeposition with self-assembled monolayers. *Chem. Phys. Lett.* **1997,** *269*, 479-484.
13. Vericat, C.; Vela, M. E.; Benitez, G.; Carro, P.; Salvarezza, R. C., Self-assembled monolayers of thiols and dithiols on gold: new challenges for a well-known system. *Chem. Soc. Rev.* **2010,** *39*, 1805-1834.
14. Nuzzo, R. G.; Allara, D. L., Adsorption of bifunctional organic disulfides on gold surfaces. *J. Am. Chem. Soc.* **1983,** *105*, 4481-4483.

15. Seitz, O.; Dai, M.; Aguirre-Tostado, F. S.; Wallace, R. M.; Chabal, Y. J., Copper−Metal Deposition on Self Assembled Monolayer for Making Top Contacts in Molecular Electronic Devices. *J. Am. Chem. Soc.* **2009,** *131*, 18159-18167.
16. Wang, C.; Wang, Z.; Zhang, X., Amphiphilic Building Blocks for Self-Assembly: From Amphiphiles to Supra-amphiphiles. *Acc. Chem. Res.* **2012,** *45*, 608-618.
17. Lu, L.; Cai, Y., Molecular Tilting and Its Impact on Frictional Properties of n-Alkane Self-Assembled Monolayers. *Langmuir* **2011,** *27*, 5953-5960.
18. Narayanan, R.; El-Sayed, M. A., Effect of Catalysis on the Stability of Metallic Nanoparticles: Suzuki Reaction Catalyzed by PVP-Palladium Nanoparticles. *J. Am. Chem. Soc.* **2003,** *125*, 8340-8347.
19. Kalliola, S.; Repo, E.; Sillanpää, M.; Singh Arora, J.; He, J.; John, V. T., The stability of green nanoparticles in increased pH and salinity for applications in oil spill-treatment. *Colloids Surf.* **2016,** *493*, 99-107.
20. Ivanova, O. S.; Zamborini, F. P., Size-Dependent Electrochemical Oxidation of Silver Nanoparticles. *J. Am. Chem. Soc.* **2010,** *132*, 70-72.
21. Pattadar, D. K.; Mainali, B. P.; Jasinski, J. B.; Zamborini, F. P., Electrooxidation, Size Stability, and Electrocatalytic Activity of 0.9 nm Diameter Gold Nanoclusters Coated with a Weak Stabilizer. *ChemElectroChem* **2020,** *7*, 800-809.
22. Kumar, A.; Buttry, D. A., Size-Dependent Anodic Dissolution of Water-Soluble Palladium Nanoparticles. *J. Phys. Chem. C* **2013,** *117*, 26783-26789.
23. Brainina, K. Z.; Galperin, L. G.; Vikulova, E. V.; Stozhko, N. Y.; Murzakaev, A. M.; Timoshenkova, O. R.; Kotov, Y. A., Gold nanoparticles electrooxidation: comparison of theory and experiment. *J. Solid State Electrochem.* **2011,** *15*, 1049-1056.
24. Pattadar, D. K.; Zamborini, F. P., Effect of Size, Coverage, and Dispersity on the Potential-Controlled Ostwald Ripening of Metal Nanoparticles. *Langmuir* **2019,** *35*, 16416-16426.
25. Steven, J. T.; Golovko, V. B.; Johannessen, B.; Marshall, A. T., Electrochemical stability of carbon-supported gold nanoparticles in acidic electrolyte during cyclic voltammetry. *Electrochim. Acta* **2016,** *187*, 593-604.
26. Mainali, B. P.; Pattadar, D. K.; Zamborini, F. P., Size-Dependent Ripening of Gold Nanoparticles through Repetitive Electrochemical Surface Oxidation-Reduction Cycling. *J. Electrochem. Soc.* **2020,** *167*, 146503-146511.
27. Tang, L.; Han, B.; Persson, K.; Friesen, C.; He, T.; Sieradzki, K.; Ceder, G., Electrochemical Stability of Nanometer-Scale Pt Particles in Acidic Environments. *J. Am. Chem. Soc.* **2010,** *132*, 596-600.
28. Pattadar, D. K.; Zamborini, F. P., Size Stability Study of Catalytically Active Sub-2 nm Diameter Gold Nanoparticles Synthesized with Weak Stabilizers. *J. Am. Chem. Soc.* **2018,** *140*, 14126-14133.
29. Ivanova, O. S.; Zamborini, F. P., Electrochemical Size Discrimination of Gold Nanoparticles Attached to Glass/Indium−Tin-Oxide Electrodes by Oxidation in Bromide-Containing Electrolyte. *Anal. Chem.* **2010,** *82*, 5844-5850.
30. Plieth, W. J., Electrochemical properties of small clusters of metal atoms and their role in the surface enhanced Raman scattering. *J. Phys. Chem.* **1982,** *86*, 3166-3170.
31. Shao-Horn, Y.; W. C. Sheng, W. C.; Chen, S.; Ferreira, P. J.; Holby, E. F.; Morgan, D., Instability of Supported Platinum Nanoparticles in Low-Temperature Fuel Cells. *Top. Catal.* **2007,** *46*, 285-305.
32. Trindell, J. A.; Clausmeyer, J.; Crooks, R. M., Size Stability and H2/CO Selectivity for Au Nanoparticles during Electrocatalytic CO2 Reduction. *J. Am. Chem. Soc.* **2017,** *139*, 16161-16167.
33. Tang, W.; Lin, H.; Kleiman-Shwarsctein, A.; Stucky, G. D.; McFarland, E. W., Size-Dependent Activity of Gold Nanoparticles for Oxygen Electroreduction in Alkaline Electrolyte. *J. Phy. Chem. C* **2008,** *112*, 10515-10519.
34. Zhou, X.; Xu, W.; Liu, G.; Panda, D.; Chen, P., Size-Dependent Catalytic Activity and Dynamics of Gold Nanoparticles at the Single-Molecule Level. *J. Am. Chem. Soc.* **2010,** *132*, 138-146.
35. Wei, W.; Chen, W., Size-dependent catalytic activity of copper nanoclusters for oxygen electroreduction in alkaline solution. *Int. J. Smart Nan. Mat.* **2013,** *4*, 62-71.

36. Gao, D.; Zhou, H.; Wang, J.; Miao, S.; Yang, F.; Wang, G.; Wang, J.; Bao, X., Size-Dependent Electrocatalytic Reduction of CO2 over Pd Nanoparticles. *J. Am. Chem. Soc.* **2015,** *137*, 4288-4291.
37. Porter, M. D.; Bright, T. B.; Allara, D. L.; Chidsey, C. E. D., Spontaneously organized molecular assemblies. 4. Structural characterization of n-alkyl thiol monolayers on gold by optical ellipsometry, infrared spectroscopy, and electrochemistry. *J. Am. Chem. Soc.* **1987,** *109*, 3559-3568.
38. Srisombat, L.; Jamison, A. C.; Lee, T. R., Stability: A key issue for self-assembled monolayers on gold as thin-film coatings and nanoparticle protectants. *Colloids Surf. A* **2011,** *390*, 1-19.
39. Giersig, M.; Mulvaney, P., Preparation of ordered colloid monolayers by electrophoretic deposition. *Langmuir* **1993,** *9*, 3408-3413.
40. Zamborini, F. P.; Crooks, R. M., Corrosion Passivation of Gold by n-Alkanethiol Self-Assembled Monolayers: Effect of Chain Length and End Group. *Langmuir* **1998,** *14*, 3279-3286.
41. Bürgi, T., Properties of the gold-sulphur interface: from self-assembled monolayers to clusters. *Nanoscale* **2015,** *7*, 15553-15567.
42. Bourg, M.-C.; Badia, A.; Lennox, R. B., Gold−Sulfur Bonding in 2D and 3D Self-Assembled Monolayers: XPS Characterization. *J. Phys. Chem. B* **2000,** *104*, 6562-6567.
43. Häkkinen, H., The gold–sulfur interface at the nanoscale. *Nature Chem.* **2012,** *4*, 443.
44. Templeton, A. C.; Wuelfing, W. P.; Murray, R. W., Monolayer-Protected Cluster Molecules. *Acc. Chem. Res.* **2000,** *33*, 27-36.
45. Kwak, K.; Lee, D., Electrochemistry of Atomically Precise Metal Nanoclusters. *Acc. Chem. Res.* **2019,** *52*, 12-22.
46. Maity, P.; Xie, S.; Yamauchi, M.; Tsukuda, T., Stabilized gold clusters: from isolation toward controlled synthesis. *Nanoscale* **2012,** *4*, 4027-4037.
47. Li, G.; Jin, R., Atomically Precise Gold Nanoclusters as New Model Catalysts. *Acc. Chem. Res.* **2013,** *46*, 1749-1758.
48. Yu, Y.; Chen, X.; Yao, Q.; Yu, Y.; Yan, N.; Xie, J., Scalable and Precise Synthesis of Thiolated Au10–12, Au15, Au18, and Au25 Nanoclusters via pH Controlled CO Reduction. *Chem. Mater.* **2013,** *25*, 946-952.
49. Brust, M.; Walker, M.; Bethell, D.; Schiffrin, D. J.; Whyman, R., Synthesis of thiol-derivatised gold nanoparticles in a two-phase Liquid–Liquid system. *J. Chem. Soc. Chem. Comm.* **1994,** 801-802.
50. San, K. A.; Shon, Y.-S., Synthesis of Alkanethiolate-Capped Metal Nanoparticles Using Alkyl Thiosulfate Ligand Precursors: A Method to Generate Promising Reagents for Selective Catalysis. *Nanomater.* **2018,** *8*, 346.
51. Parker, J. F.; Fields-Zinna, C. A.; Murray, R. W., The Story of a Monodisperse Gold Nanoparticle: Au25L18. *Acc. Chem. Res.* **2010,** *43*, 1289-1296.
52. Negishi, Y.; Takasugi, Y.; Sato, S.; Yao, H.; Kimura, K.; Tsukuda, T., Kinetic Stabilization of Growing Gold Clusters by Passivation with Thiolates. *J. Phy. Chem. B* **2006,** *110*, 12218-12221.
53. Mazloomi-Rezvani, M.; Salami-Kalajahi, M.; Roghani-Mamaqani, H.; Pirayesh, A., Effect of surface modification with various thiol compounds on colloidal stability of gold nanoparticles. *Appl. Organometal. Chem.* **2018,** *32*, 4079-4090.
54. Gao, J.; Huang, X.; Liu, H.; Zan, F.; Ren, J., Colloidal Stability of Gold Nanoparticles Modified with Thiol Compounds: Bioconjugation and Application in Cancer Cell Imaging. *Langmuir* **2012,** *28*, 4464-4471.
55. Borzenkov, M.; Chirico, G.; D'Alfonso, L.; Sironi, L.; Collini, M.; Cabrini, E.; Dacarro, G.; Milanese, C.; Pallavicini, P.; Taglietti, A.; Bernhard, C.; Denat, F., Thermal and Chemical Stability of Thiol Bonding on Gold Nanostars. *Langmuir* **2015,** *31*, 8081-8091.
56. Park, J.-W.; Shumaker-Parry, J. S., Strong Resistance of Citrate Anions on Metal Nanoparticles to Desorption under Thiol Functionalization. *ACS Nano* **2015,** *9*, 1665-1682.
57. McCue, I.; Snyder, J.; Li, X.; Chen, Q.; Sieradzki, K.; Erlebacher, J., Apparent Inverse Gibbs-Thomson Effect in Dealloyed Nanoporous Nanoparticles. *Phys. Rev. Lett.* **2012,** *108*, 225503.
58. Pattadar, D. K.; Sharma, J. M.; Mainali, B. P.; Zamborini, F. P., Anodic Stripping Electrochemical Analysis of Metal Nanoparticles. *Curr. Opin. Electrochem.* **2019,** *13*, 147-156.

59. Hostetler, M. J.; Murray, R. W., Colloids and Self-Assembled Monolayers. *Curr. Opin. Colloid Interface Sci.* **1997,** *2*, 42-50.
60. Zanchet, D.; Tolentino, H.; Martins Alves, M. C.; Alves, O. L.; Ugarte, D., Inter-atomic distance contraction in thiol-passivated gold nanoparticles. *Chem. Phys. Lett.* **2000,** *323*, 167-172.
61. Vericat, C.; Benitez, G. A.; Grumelli, D. E.; Vela, M. E.; Salvarezza, R. C., Thiol-capped gold: from planar to irregular surfaces. *J. Phys. Condens. Matter* **2008,** *20*, 184004.
62. Cortés, E.; Rubert, A. A.; Benitez, G.; Carro, P.; Vela, M. E.; Salvarezza, R. C., Enhanced Stability of Thiolate Self-Assembled Monolayers (SAMs) on Nanostructured Gold Substrates. *Langmuir* **2009,** *25*, 5661-5666.
63. Pattadar, D. K.; Sharma, J. N.; Mainali, B. P.; Zamborini, F. P., Impact of the Assembly Method on the Surface Area-to-Volume Ratio and Electrochemical Oxidation Potential of Metal Nanospheres. *J. Phys. Chem. C* **2019,** *123*, 24304-24312.
64. Sharma, J. N.; Pattadar, D. K.; Mainali, B. P.; Zamborini, F. P., Size Determination of Metal Nanoparticles Based on Electrochemically Measured Surface-Area-to-Volume Ratios. *Anal. Chem.* **2018,** *90*, 9308-9314.
65. Jana, N. R.; Gearheart, L.; Murphy, C. J., Wet Chemical Synthesis of High Aspect Ratio Cylindrical Gold Nanorods. *J. Phy. Chem. B* **2001,** *105*, 4065-4067.
66. Turkevich, J.; Stevenson, P. C.; Hillier, J., A study of the nucleation and growth processes in the synthesis of colloidal gold. *Discuss. Faraday. Soc.* **1951,** *11*, 55-75.
67. Liu, X.; Xu, H.; Xia, H.; Wang, D., Rapid Seeded Growth of Monodisperse, Quasi-Spherical, Citrate-Stabilized Gold Nanoparticles via H2O2 Reduction. *Langmuir* **2012,** *28*, 13720-13726.
68. Jacob, J. D. C.; Lee, T. R.; Baldelli, S., In Situ Vibrational Study of the Reductive Desorption of Alkanethiol Monolayers on Gold by Sum Frequency Generation Spectroscopy. *J Phy. Chem. C* **2014,** *118*, 29126-29134.
69. Elliott, E. W.; Glover, R. D.; Hutchison, J. E., Removal of Thiol Ligands from Surface-Confined Nanoparticles without Particle Growth or Desorption. *ACS Nano* **2015,** *9*, 3050-3059.